Energy based modeling of ionic polymer metal composite actuators dedicated to the control of flexible structures

Ning Liu, *Student member, IEEE,* Yongxin Wu, *Member, IEEE,* Yann Le Gorrec, *Senior Member, IEEE*

***Abstract*—This paper deals with the control-oriented energy-based modeling of ionic polymer metal composite patches using multiscale infinite dimensional port-Hamiltonian formulations and Lagrange multipliers. Inspired by the work of Gou Nishida *et al.* 2012, but considering different assumptions, this paper focuses on the constraints arising from the coupling between the polymer gel and the compliant mechanical structure of the actuator, under the quasi-static mechanical assumption for the gel, leading to a constrained port Hamiltonian system. The geometric structure of the overall system and the associated energy balance are derived. The proposed energy-based model of the IPMC actuator allows deriving controllers via energy-based control design methods with a clear physical interpretation. The proposed actuator model is further discretized in space using a structure preserving finite difference method. The Lagrange multipliers are eliminated using coordinate projections. Simulations are compared with experimental results. With proper discretization numbers, our model is consistent with the physical system. Finally, Lagrange multipliers are exploited to connect the actuator to a 2-dimensional flexible structure stemming from the modeling of a flexible endoscope.**

***Index Terms*—IPMC actuator, infinite dimensional port Hamiltonian system, 2D shell modeling, model discretization.**

I. Introduction

IONIC polymer metal composites (IPMCs) are widely used as actuators or/and sensors in biomedical and industrial domains [1], [2], due to their advantages of low-cost voltage, large deformation, as well as broad bandwidth in comparison with piezoelectric materials.

IPMCs are composed of an electroactive polymer (polyelectrolyte gel) whose surfaces are coated with a conductor such as gold. The working principle is the following: cations and solvent molecules in the gel transport to the cathode side of the electrode when an electrical potential difference is imposed across the two boundaries of the double layer. As a consequence, the cathode side swells and the anode side shrinks, entailing a bending effect to the anode side [3].

Based on the aforementioned physical structure and working principle, various models of such actuators have been proposed in the literature, mainly sorted into three subclasses: black box models, white box models and grey box models.

This work has been supported by the French-German ANR-DFG INFIDHEM project (contract: ANR-16-CE92-0028), the EIPHI Graduate School (contract ANR-17-EURE-0002). The second author acknowledges the Bourgogne-Franche-comté Region ANER 2018Y-06145. The third author has received founding from the European Commision Marie Skłodowska-Curie Fellowship, ConFlex ITN Network (Reference code: 765579).

Ning Liu, Yongxin Wu, Yann Le Gorrec are with the FEMTO-ST institute, UMR CNRS 6174, département AS2M, Université Bourgogne Franche-Comté/ ENSMM, F-25000 Besançon, France (e-mail: respectively, ning.liu, yongxin.wu@femto-st.fr, and yann.le.gorrec@ens2m.fr).

As initially proposed in [4], [5], the black box model, which is purely empirical and which focuses only on the relation between specific inputs and outputs (e.g. voltage and tip displacement of the IPMC), is simple to establish [6]. However, as it is based on strong assumptions, it cannot be applied to all types of IPMC, nor to different boundary or experimental conditions. In contrast to the previous one, the white box model is established via principles of physics and chemistry at the molecular level [7]–[9], resulting in a set of partial differential equations (PDEs). The complexity of such model makes it difficult to handle from a numerical point of view and difficult to be validated experimentally.

Different from the two previous models, the grey box model has been investigated in [10]–[12]. It is formulated according to physical principles in conjunction with simplified assumptions and parameter identifications. It is proven that this kind of model presents a higher accuracy and wider universality than the black box model. Meanwhile, it is more preferable than its white counterpart in terms of the numerical implementation and the experimental validation. According to the composition of IPMCs, the model is derived considering three subsystems: the interface between the gel and the electrode, the polymer and the mechanical structure. In [12] a control-oriented and physical-based model of an IPMC actuator using an infinite dimensional transfer function between the input voltage and the output endpoint displacement of the actuator is proposed. The mechanical dynamics is approximated by a second-order system, which is valid only at low frequencies. With the model reduction of the infinite dimensional transfer function, an H_∞ controller is implemented. This work focuses on the modeling and control design of a single actuator in a given range of frequencies.

The proposed approach is different as it aims at providing a model of IMPC patches suitable for distributed control of flexible structures. The proposed model has then to cope with higher frequency modes and to be easy to interconnect with both elastic beams and thin shell models, the control design being derived using energy based control design methods in order to have a better physical interpretation for the controller. Recently, a new type of grey box model has been proposed in [13] within the framework of port-Hamiltonian systems (PHSs). This port based modeling expresses the dynamics of the system through energy exchanges between its subcomponents. As a result, it is particularly well suited for the modeling of complex, multiphysical and multiscale systems via power preserving interconnections. Yet, due to the

considered assumptions, the model proposed in [13] presents some important limitations. In [13] a local homogeneity assumption is considered for the polymer deformation. The multiscale coupling of the gel with the mechanical structure is done through the bending moment, locally defined for the polymer gel, and the structure deformation, globally defined for the mechanical structure. Furthermore the polymer action is seen as modifying the internal properties of the mechanical structure. As a consequence singularities may appear when the mechanical deformation is homogeneous. In this case, due to the considered assumptions, the bending moment provided by the polymer gel is homogeneous and without any effect on the distributed mechanical structure. On the other hand, the coupling between the mechanical properties of the gel (considered as quasi-static) and the mechanical properties of the actuator structure in [13] is implicit, with conflicting causalities in the proposed Bond Graph. In this paper we make the quasi-static behavior of the gel explicit and express the algebraic constraint arising from the coupling between the gel and the mechanical structure of the actuator with a Lagrange multiplier. We also consider the action of the polymer gel on the mechanical structure as an external distributed bending moment, avoiding singularities associated with homogeneous deformations. The discretization of the proposed IPMC model is structure preserving, such that our discretized model is again a port-Hamiltonian system. To go much further, a similar strategy using Lagrangian multipliers is used to connect this IPMC model to a 2-dimensional (2D) elastic tube stemming from the modeling of a flexible endoscope.

The paper is organized as follows. Section II establishes the energy based model of the IPMC as a modular composition of three subsystems and their multiscale coupling under the port-Hamiltonian framework. The overall structure of the system and the associated energy balance are made explicit. In Section III, the finite difference method on staggered grids is applied to discretize the IPMC model in a structure preserving way. Meanwhile, the Lagrange multipliers are eliminated by projection. Comparisons between simulated and experimental results are given in Sections IV. In Section V is proposed the model of a 2D flexible structure stemming from the modeling of a flexible endoscope actuated by an IPMC patch. In Section VI are given conclusions and perspectives.

II. Modeling of the IPMC actuator

The IPMC patch under investigation is of length L, width b and thickness h. Its shape and structure are depicted in Fig. 1.

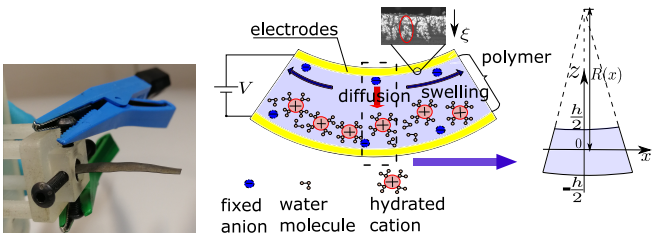

(a) IPMC patch. (b) IPMC structure [14].

Fig. 1: Shape and structure of an IPMC actuator patch.

This IPMC model is composed of three subsystems: the electrical system stemming from the modeling of the electrode/polymer interface, the electro-stress diffusion system stemming from the modeling of the polymer, and the mechanical system stemming from the modeling of the overall mechanical structure deformation, which are at scales of nanometer, micrometer and centimeter [13], respectively. In this section, the different subsystems and the way they are coupled are discussed. The main differences with the model proposed in [13] lie in the electro-stress diffusion and mechanical models and the way they are interconnected (cf. subsections B, C, D).

A. Electrical system

Starting with the electrical part, we assume that the voltage V is uniformly distributed on the double layers. According to [13], each fractal-like structure on two electrodes is referenced as a virtual coordinate $\xi \in [0, L_\xi]$ as marked by a red circle in Fig. 1b, and is represented by a distributed RC circuit illustrated in Fig. 2. For each structure, there are innumerable infinitesimal branches, where $R_1(\xi)$ represents the resistance density between two adjacent branches, and $R_2(\xi)$ and $C_2(\xi)$ correspond to the resistive and capacitive impedance densities of each branch, respectively. By taking the variables: $f_1(\xi,t) = -\partial Q(\xi,t)/\partial t$,

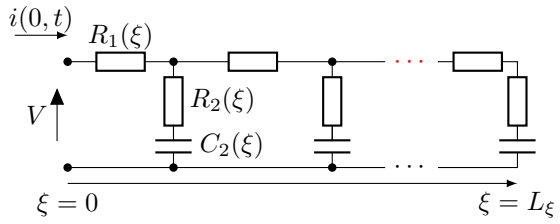

Fig. 2: Infinite dimension electrical system.

$e_1(\xi,t) = Q(\xi,t)/C_2(\xi) + R_2(\xi)\partial Q(\xi,t)/\partial t$, $f_{r1}(\xi,t) = \partial/\partial\xi\,(Q(\xi,t)/C_2(\xi) + R_2(\xi)\partial Q(\xi,t)/\partial t)$, where $Q(\xi,t)$ is the charge density of each capacitor, one can express the dynamic function of the circuit in a PHS form: [1]

$$\begin{pmatrix} f_1 \\ f_{r1} \end{pmatrix} = \begin{pmatrix} 0 & \partial_\xi \\ \partial_\xi & 0 \end{pmatrix} \begin{pmatrix} e_1 \\ e_{r1} \end{pmatrix}, \text{with } e_{r1}(\xi,t) = -\frac{f_{r1}(\xi,t)}{R_1(\xi)}. \quad (1)$$

Assuming that the impedance is infinite, the current at the endpoint of each fractal structure is zero, namely $e_{r1}(L_\xi) = 0$.

According to [15] and [16], the boundary port variables of (1) can be expressed with respect to the physical boundary conditions:

$$\begin{aligned} \begin{pmatrix} f_{\partial\xi}^T & e_{\partial\xi}^T \end{pmatrix}^T &= \begin{pmatrix} e_1(0) & e_1(L_\xi) & -e_{r1}(0) & e_{r1}(L_\xi) \end{pmatrix}^T \\ &= \begin{pmatrix} V + V_c & e_1(L_\xi) & -I_e & 0 \end{pmatrix}^T, \end{aligned} \quad (2)$$

where V_c corresponds to the voltage coming from the gel, and I_e represents the output current.

The Hamiltonian reads $H_{el} = \int_\xi Q^2/(2C_2)\,\mathrm{d}\xi$. The energy balance equation is given by:

$$\frac{\partial H_{el}}{\partial t} = \int_\xi \frac{\partial Q}{\partial t}^T \frac{Q}{C_2}\,\mathrm{d}\xi \le f_{\partial\xi}^T e_{\partial\xi}, \quad (3)$$

[1]For the sake of compactness, $\partial/\partial\xi$ is denoted as ∂_ξ and the symbol t is omitted in the following context.

where we have used the integration by parts, (2) and the dissipation arising from R_1 and R_2.

B. Electro-stress diffusion system

In this part we are interested into the electro-physical properties of the polymer and the associated electro-stress diffusion process occurring in the gel. The gel is composed of a solid and a liquid phase. The former contains the polymer network and fixed anions, and the latter includes cations and water molecules [17]. In the liquid phase, two coupled phenomena can be distinguished: the electro-osmosis and the water transport [18]. This will later be modeled using P.G. de Gennes' method [19]. The solid phase is assumed to be at a pseudo-equilibrium state, because the solvent dynamics is much slower compared to the mechanical dynamics of the polymer, hence forming a quasi-static electro-stress diffusion coupling model [13], [18].

This assumption makes the mechanical dynamics of the gel implicit, such that the radius of curvature of the gel is addressed with the help of the rotational angle of the patch deformation along the x coordinate, i.e. $1/R(x) = -\partial\theta(x)/\partial x$, which leads to **algebraic constraints** in the coupling between the electro-stress diffusion system and the mechanical system associated with the patch deformation.

Here we explain both the solid phase and the liquid phase modelings in details. The deformation of the solid phase is assumed to be symmetric (right graph in Fig. 1b). The curvature $R(x)$ is assumed to be *locally homogeneous* along the x direction. Stress tensors are formulated by the curvature $R(x)$ and the swelling ratio $f_s(z,x)$:

$$\sigma_{xx}(z,x) = \left(K - \frac{2}{3}G\right) f_s(z,x) + \frac{2G}{R(x)} z,$$
$$\sigma_{zz}(z,x) = \left(K + \frac{4}{3}G\right) f_s(z,x) - \frac{4G}{R(x)} z,$$

where K and G are the bulk and shear modulus of the gel, respectively [18].

The pseudo-equilibrium state of the gel gives the pressure p as

$$p = \sigma_{zz}. \tag{4}$$

In the liquid phase, it is supposed that the gel goes only in the z direction. This is consistent with the hypothesis of local homogeneity of $R(x)$ in the solid phase. The conservation law on the volume leads to [18]:

$$\frac{\partial f_s(z,x)}{\partial t} = -\frac{\partial \mathbf{j}_s(z,x)}{\partial z}, \tag{5}$$

where $\mathbf{j}_s(z,x)$ is the flux of solvent.

Different physical models dealing with the coupling between the ion and water transport have been studied, among which are the ones developed by Nemat-Nasser [8] and by P.G. de Gennes [19]. The former one [8] emphasizes the importance of the electrostatic force over the hydraulic force and the latter [19] considers that the hydraulic force prevails in the coupling. Both models are consistent with the experimental results. In this paper we use the P.G. de Gennes' model because it is based on irreversible thermodynamics and is well suited for the port-Hamiltonian formulation, leading to a natural definition of the power conjugated flow and effort variables. The model is formulated as follows:

$$\mathbf{j}_e = -\sigma_e \nabla\psi - \lambda\nabla p,\ \mathbf{j}_s = -\phi\frac{d^2}{\eta}\nabla p - \lambda\nabla\psi, \tag{6}$$

where $\mathbf{j}_e$ represents the electrical current density. σ_e is the conductance, λ stands for the Onsager's coupling constant and ψ is the electric field. ϕ, d and η denote the water volume fraction, the effective pore size and the water viscosity, respectively, whose product $\phi d^2/\eta$ forms the constant of the Darcy's permeability [19].

By combining (4) and (6), one gets:

$$\begin{aligned}\mathbf{j}_s(z) &= \frac{\lambda}{\sigma_e}\mathbf{j}_e + \left(\frac{\lambda^2}{\sigma_e} - \phi\frac{d^2}{\eta}\right)\frac{\partial p}{\partial z} \\ &= -\mathcal{R}_g\frac{\partial}{\partial z}\left(\mathcal{R}_f f_s(z,x)\right) + \mathbb{1}_Z\frac{\lambda}{\sigma_e}\mathbf{j}_e + \mathbb{1}_Z\Phi(x),\end{aligned} \tag{7}$$

with $\mathcal{R}_g = d\left(\phi/\eta - \lambda^2/\left(d^2\sigma_e\right)\right)$, $\mathcal{R}_f = d\left(K + 4/3G\right)$, and $\Phi(x) = \left(\phi d^2/\eta - \lambda^2/\sigma_e\right)4G/R(x)$. $\mathcal{R}_f f_s$ can be seen analogous to a compression force. $\mathbb{1}_Z$ is firstly proposed in [13] and serves for the multiscale coupling. It stands for the characteristic function of domain z, and distributes uniformly the boundary values $\frac{\lambda}{\sigma_e}\mathbf{j}_e$ and $\Phi(x)$ into the z domain.

Similar to the electrical system, by defining $f_2 = -\partial_t f_s$, $f_{r2} = \mathcal{R}_f\partial_z f_s$, $e_2 = \mathcal{R}_f f_s$ and $e_{r2} = -\mathcal{R}_g\partial_z\left(\mathcal{R}_f f_s\right)$, (5) and (7) can then be reformulated in the port-Hamiltonian framework as:

$$\begin{pmatrix} f_2 \\ f_{r2}\end{pmatrix} = \begin{pmatrix} 0 & \partial_z \\ \partial_z & 0\end{pmatrix}\begin{pmatrix} e_2 \\ e_{r2}\end{pmatrix}, \text{with } e_{r2} = -\mathcal{R}_g f_{r2}. \tag{8}$$

The boundary variables are:

$$\begin{pmatrix} f_{\partial z} \\ e_{\partial z}\end{pmatrix} = \begin{pmatrix} e_{r2}\left(-\frac{h}{2}\right) & e_{r2}\left(\frac{h}{2}\right) & -e_2\left(-\frac{h}{2}\right) & e_2\left(\frac{h}{2}\right)\end{pmatrix}^T. \tag{9}$$

Boundary conditions come from the impermeable assumption that $\mathbf{j}_s(\pm h/2) = 0$ [13]. The Hamiltonian associated with the electro-stress diffusion system is $H_{em} = \int_z \mathcal{R}_f f_s^2/2\,\mathrm{d}z$. The energy balance equation is formulated as $\partial_t H_{em} = \int_z \left(\partial_t f_s \cdot \mathcal{R}_f f_s\right)\mathrm{d}z \le f_{\partial z}^T e_{\partial z}$, which is similar to the energy balance equation (3).

Considering that the swelling and shrinking are visualized at a macro scale, the gel generates locally a bending moment in the x direction,:

$$\begin{aligned}M(x) &= \int_z (\sigma_{xx} - p)\, bz\,\mathrm{d}z \\ &= \int_z B_a\mathcal{R}_f f_s(z,x)\,\mathrm{d}z + \frac{Gbh^3}{2R(x)},\end{aligned} \tag{10}$$

with $B_a(z) = -2Gbz/\mathcal{R}_f$. This bending moment can later be divided into two parts, M_{x1} and M_{x2}, reading:

$$M_{x1}(x) = \int_z B_a\mathcal{R}_f f_s(z,x)\,\mathrm{d}z,\ M_{x2}(x) = \frac{Gbh^3}{2R(x)}.$$

C. Mechanical system

A slightly deformed IPMC actuator can be modeled as a Timoshenko beam with $x \in [0, L]$ under the port Hamiltonian framework [20]:

$$\begin{pmatrix} f_3 \\ f_4 \\ f_5 \\ f_6 \end{pmatrix} = \begin{pmatrix} 0 & \partial_x & 0 & -1 \\ \partial_x & 0 & 0 & 0 \\ 0 & 0 & 0 & \partial_x \\ 1 & 0 & \partial_x & 0 \end{pmatrix} \begin{pmatrix} e_3 \\ e_4 \\ e_5 \\ e_6 \end{pmatrix} + \begin{pmatrix} 0 \\ 0 \\ 0 \\ 1 \end{pmatrix} \frac{M}{L}(x,t), \quad (11)$$

where [2] $f_3 = -(\partial_{tx}\omega - \partial_t\theta)$, $f_4 = \rho A \partial_{tt}\omega$, $f_5 = -\partial_{tx}\theta$, $f_6 = \rho I \partial_{tt}\theta$, $e_3 = GA(\partial_x\omega - \theta)$, $e_4 = -\partial_t\omega$, $e_5 = EI\partial_x\theta$ and $e_6 = -\partial_t\theta$. ω denotes the longitudinal displacement, ρ is the beam density, E represents the Young's modulus, A stands for the cross section area of the beam, I is the moment of inertia, and $M(x,t)$ is the distributed bending moment coming from the gel, formulated by (10).

The boundary port variables are calculated as:

$$\begin{pmatrix} f_{\partial x} \\ e_{\partial x} \end{pmatrix} = \begin{pmatrix} \begin{pmatrix} e_4(0) & e_3(L) & e_6(0) & e_5(L) \end{pmatrix}^T \\ \begin{pmatrix} -e_3(0) & e_4(L) & -e_5(0) & e_6(L) \end{pmatrix}^T \end{pmatrix}. \quad (12)$$

The Hamiltonian of the beam is $H_m = \frac{1}{2}\int_x \left(GA(\partial_x\omega - \theta)^2 + EI\partial_x^2\theta + \rho A\partial_t^2\omega + \rho I\partial_t^2\theta\right) \mathrm{d}x$.

Remark 1. *Differently from [13] the quasi-static behavior of the polymer is made explicit in the electro-stress diffusion system and the contribution of the polymer on the mechanical structure stemming from the modeling of the patch bending is considered as a distributed source term.*

D. Coupling between the different subsystems

1) Electrical / electro-stress diffusion systems: According to (7), the interconnection between the electrical system and the electro-stress diffusion system is made through the boundary variables $e_1(0)$, $e_{r1}(0)$, and $\mathbf{j}_s(\pm h/2)$. Given that these boundary variables are of different scales and are defined in different independent domains ξ and z, a coupling element, named boundary multiscale coupling (BMS), has been introduced in [13] to proceed with the interconnection. As depicted

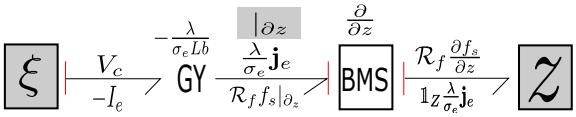

Fig. 3: Bond graph of the coupling between ξ and z, with $\mathcal{R}_f f_s|_{\partial z} = \mathcal{R}_f\left(f_s\left(\frac{h}{2}\right) - f_s\left(-\frac{h}{2}\right)\right)$.

in the bond graph in Fig. 3, the BMS element works as a differential gyrator. By crossing it, $\frac{\lambda}{\sigma_e}\mathbf{j}_e$ is multiplied by the characteristic function $\mathbb{1}_Z$, which represents a uniform distributed input in the domain z. Conversely, the effort variable $\partial(\mathcal{R}_f f_s)/\partial z$ in the z domain goes through the BMS in order to be integrated over z and become $\mathcal{R}_f\left(f_s\left(\frac{h}{2}\right) - f_s\left(-\frac{h}{2}\right)\right)$. The current density $\mathbf{j}_e$ is related to the current I_e by

$$\mathbf{j}_e = \frac{I_e}{Lb}. \quad (13)$$

[2]The second-order derivative operator $\partial^2/(\partial x \partial y)$ is denoted by ∂_{xy}.

Based on the power conservation, $\mathcal{R}_f f_s|_{\partial z}$ is transformed into the voltage V_c via the gyrator GY:

$$V_c = -\frac{\lambda}{\sigma_e Lb}\mathcal{R}_f\left(f_s\left(\frac{h}{2}\right) - f_s\left(-\frac{h}{2}\right)\right). \quad (14)$$

2) Electro-stress diffusion system / mechanical system: At the macro-scale, the electro-stress diffusion model connects with the mechanical model through two bending moments (M_{x1} and M_{x2}) and the angular velocity $\partial\theta(x,t)/\partial t$.

The bond graph of the interconnection through $M_{x1}(x)$ is shown in Fig. 4 (left column). An additional term $\frac{B_a}{L}\mathbb{1}_Z\frac{\partial\theta}{\partial t}$ is added into (5) to match the power conservation. This term is considered in the electro-stress diffusion system as a source term coming from the mechanical level:

$$\frac{\partial f_s(z,x)}{\partial t} = -\frac{\partial \mathbf{j}_s(z)}{\partial z} - \frac{B_a}{L}\mathbb{1}_Z\frac{\partial\theta(x)}{\partial t}.$$

The coupling through $M_{x2}(x)$ and $\Phi(x)$ aims at describing the aforementioned algebraic constraints. From the bond graph in Fig. 4, since $\Phi(x)$ acts as a flow source for the electro-stress diffusion system and $M_{x2}(x)$ is the output of this system, with the linear relation

$$M_{x2}(x) = \Phi(x)B_p, \text{with } B_p = \frac{bh^3}{4}\left(\phi\frac{d^2}{\eta} - \frac{\lambda^2}{\sigma_e}\right)^{-1}, \quad (15)$$

a Lagrange multiplier $\lambda_{\mathbf{L}}$ is added to express the associated constraint and to guarantee the causality of the system, as presented on the right column of Fig. 4. One gets:

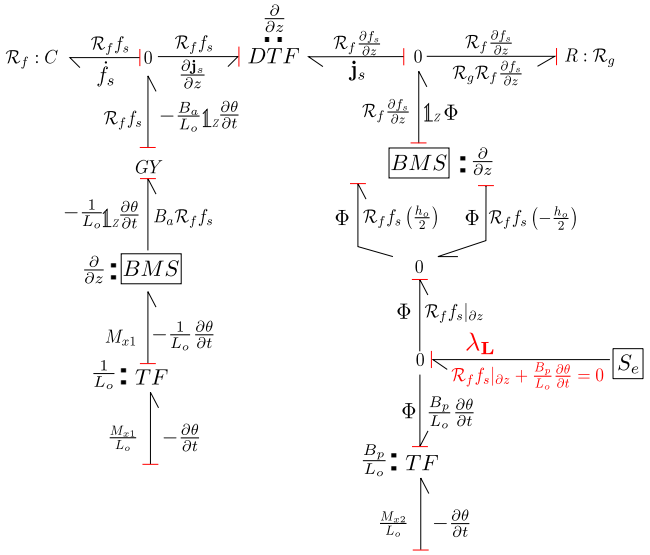

Fig. 4: Bond graph of the coupling between z and x, through M_{x1} (left column), M_{x2} (right column) and $\partial\theta/\partial t$.

$$\begin{pmatrix} 1 & \frac{B_p}{L} \end{pmatrix}^T \lambda_{\mathbf{L}} = \begin{pmatrix} \Phi & \frac{M_{x2}}{L} \end{pmatrix}^T. \quad (16)$$

Furthermore, the physical constraint associated with the Lagrange multiplier $\lambda_{\mathbf{L}}$ is given by:

$$\begin{pmatrix} 1 & \frac{B_p}{L} \end{pmatrix} \begin{pmatrix} \mathcal{R}_f f_s|_{\partial z} \\ \frac{\partial\theta}{\partial t} \end{pmatrix} = \mathcal{R}_f f_s|_{\partial z} + \frac{B_p}{L}\frac{\partial\theta}{\partial t} = 0. \quad (17)$$

It reveals that the arrow associated with the Lagrange multiplier in the bond graph (shown in Fig. 4) is an effort

source with zero flow, such that by passing the '0' junction, the effort variable Φ remains unchanged, while the flow variables $\mathcal{R}_f f_s|_{\partial z}$ and $\frac{B_p}{L}\frac{\partial \theta}{\partial t}$ sum to zero, ensuring the power conservation. This is analogous to an interconnection of two glued mass-spring systems, where the two masses have the same velocity and inverse reaction forces. Accordingly, (8) changes to:

$$\begin{pmatrix} f_2 \\ f_{r2} \end{pmatrix} = \begin{pmatrix} 0 & \partial_z \\ \partial_z & 0 \end{pmatrix} \begin{pmatrix} e_2 \\ e_{r2} \end{pmatrix} + \begin{pmatrix} \frac{B_a}{L}\mathbb{1}_Z \frac{\partial \theta}{\partial t} + \partial_z \mathbb{1}_Z \lambda_{\mathbf{L}} \\ 0 \end{pmatrix}, \quad (18)$$

closed with $e_{r2} = -\mathcal{R}_g f_{r2}$, boundary variables (9), and interconnections (16) and (17).

E. The overall system

The three above subsystems (1), (18) and (11), as well as their boundary variables (2), (9), and (12), can be coupled through the relations (13), (14) and the Lagrange multiplier (16) and (17), to get the global system:

$$f = \mathcal{J} e + \mathbf{A_L} \lambda_{\mathbf{L}}, \quad (19)$$

with $f = \begin{pmatrix} f_1 & f_{r1} & f_2 & f_{r2} & f_3 & f_4 & f_5 & f_6 \end{pmatrix}^T$,
$e = \begin{pmatrix} e_1 & e_{r1} & e_2 & e_{r2} & e_3 & e_4 & e_5 & e_6 \end{pmatrix}^T$,

$$\mathcal{J} = \begin{pmatrix} 0 & \partial_\xi & 0 & 0 & 0 & 0 & 0 & 0 \\ \partial_\xi & 0 & 0 & 0 & 0 & 0 & 0 & 0 \\ 0 & 0 & 0 & \partial_z & 0 & 0 & 0 & -\frac{B_a}{L}\mathbb{1}_Z \\ 0 & 0 & \partial_z & 0 & 0 & 0 & 0 & 0 \\ 0 & 0 & 0 & 0 & 0 & \partial_x & 0 & -1 \\ 0 & 0 & 0 & 0 & \partial_x & 0 & 0 & 0 \\ 0 & 0 & 0 & 0 & 0 & 0 & 0 & \partial_x \\ 0 & 0 & \int_Z \frac{B_a}{L}(\cdot)dz & 0 & 1 & 0 & \partial_x & 0 \end{pmatrix},$$

and $\mathbf{A_L}^* = \begin{pmatrix} 0 & 0 & (\cdot)|_{\frac{h}{2}} - (\cdot)|_{-\frac{h}{2}} & 0 & 0 & 0 & 0 & -\frac{B_p}{L} \end{pmatrix}$, such that

$$\mathbf{A_L}^* e = e_2\left(\frac{h}{2}\right) - e_2\left(-\frac{h}{2}\right) - \frac{B_p}{L} e_6 = 0, \quad (20)$$

which is similar to the constraint (17). The *extended space of flow variables* is defined as $\bar{\mathscr{F}} = \mathscr{F} \times \mathscr{F}_\partial$, with:

$$\begin{aligned} \mathscr{F} &= \mathscr{F}_{(0,L_\xi)} \times \mathscr{F}_{(-\frac{h}{2},\frac{h}{2})} \times \mathscr{F}_{(0,L)} \\ &= L_2\left([0,L_\xi]\times[0,L],\mathbb{R}^2\right) \times L_2\left([-\frac{h}{2},\frac{h}{2}]\times[0,L],\mathbb{R}^2\right) \\ &\quad \times L_2\left([0,L],\mathbb{R}^4\right), \end{aligned}$$

$$\mathscr{F}_\partial = \mathscr{F}_{\partial\xi} \times \mathscr{F}_{\partial z} \times \mathscr{F}_{\partial x} = \mathbb{R}^2 \times \mathbb{R}^2 \times \mathbb{R}^4.$$

Let $H^N((a,b);R^n)$ denote the Sobolev space on the interval (a,b). The *extended space of effort variables* is $\bar{\mathscr{E}} = \mathscr{E} \times \mathscr{E}_\partial$, with:

$$\begin{aligned} \mathscr{E} &= \mathscr{E}_{(0,L_\xi)} \times \mathscr{E}_{(-\frac{h}{2},\frac{h}{2})} \times \mathscr{E}_{(0,L)} \\ &= H^1\left([0,L_\xi]\times[0,L],\mathbb{R}^2\right) \times H^1\left([-\frac{h}{2},\frac{h}{2}]\times[0,L],\mathbb{R}^2\right) \\ &\quad \times H^1\left([0,L],\mathbb{R}^4\right), \end{aligned}$$

$$\mathscr{E}_\partial = \mathscr{E}_{\partial\xi} \times \mathscr{E}_{\partial z} \times \mathscr{E}_{\partial x} = \mathbb{R}^2 \times \mathbb{R}^2 \times \mathbb{R}^4.$$

Proposition. *The linear subset $\mathscr{D} \in \bar{\mathscr{F}} \times \bar{\mathscr{E}}$ defined by*

$$\begin{aligned} \mathscr{D} = \Bigg\{ \begin{pmatrix} f \\ f_\partial \\ e \\ e_\partial \end{pmatrix} \Bigg| & f \in \mathscr{F}, e \in \mathscr{E}, \begin{pmatrix} f_\partial \\ e_\partial \end{pmatrix} \in \mathscr{F}_\partial \times \mathscr{E}_\partial, \\ & f = \mathcal{J} e + \mathbf{A_L}\lambda_{\mathbf{L}}, \mathbf{A_L}^* e = 0, \lambda_{\mathbf{L}} \in H^1([0,L],\mathbb{R}), \\ & e_1(0) + \frac{\lambda}{\sigma_e L b}\left(e_2\left(\frac{h}{2}\right) + e_2\left(-\frac{h}{2}\right)\right) = V, \\ & e_{r2}\left(\pm\frac{h}{2}\right) + \frac{\lambda}{\sigma_e L b} e_{r1}(0) + \lambda_{\mathbf{L}} = 0, \\ & e_{r1}(L_\xi) = e_3(L) = e_4(0) = e_5(L) = e_6(0) = 0 \Bigg\} \end{aligned}$$

is a modulated Stokes-Dirac structure.

Proof: Equation (19) together with (20) can be reformulated as :

$$\begin{pmatrix} f \\ 0 \end{pmatrix} = \underbrace{\begin{pmatrix} \mathcal{J} & \mathbf{A_L} \\ \mathbf{A_L}^* & 0 \end{pmatrix}}_{\mathcal{J}_e} \begin{pmatrix} e \\ \lambda_{\mathbf{L}} \end{pmatrix},$$

The modulated Stokes-Dirac structure is inherent to the skew symmetry of $\mathcal{J}_e$. The skew symmetry of $\mathcal{J}_e$ lies in the equality between $\langle e^1, \mathcal{J}_e e^2\rangle$ and $\langle -\mathcal{J}_e e^1, e^2\rangle$ with the input, where $\langle\cdot,\cdot\rangle$ denotes the inner product in the Hilbert space. e^1 and e^2 are two pairs of effort variables in $\mathscr{E}$. Using integration by parts, relations of interconnection and boundary conditions II-E defined in $\mathscr{D}$, we have

$$\langle e^1, \mathcal{J}_e e^2\rangle = \langle -\mathcal{J}_e e^1, e^2\rangle - V\int_x \left(e^2_{r1}(0) + e^1_{r1}(0)\right) \mathrm{d}x,$$

where $-\int_x e^2_{r1}(0)dx$ is the output current I_{total} along the IPMC electrodes. ■

III. Multiscale discretization of the IPMC actuator

We consider now the discretization of the IPMC actuator model (19). To preserve the port Hamiltonian structure of the system, which is important for both analysis and control design, the structure preserving finite difference method on staggered grids [21] is applied for the discretization in space. In what follows, ξ and z are local coordinates, while x is the global coordinate, which rises the assumption that each point in x possesses one corresponding ξ and z. As a result, there are $N_e\,(= N_\xi \times N_b)$ elements for the electrical system, $N_g\,(= N_z \times N_b)$ elements for the electro-stress diffusion system, and N_b elements for the mechanical system.

A. Discretization of the electrical system

Before starting the discretization, (1) has to be reformulated in order to handle its algebraic linear expression in e_1. Therefore, (1) is rewritten as:

$$\begin{pmatrix} f_1 \\ f_{r1} \\ f_1 \end{pmatrix} = \begin{pmatrix} 0 & \partial_\xi & 0 \\ \partial_\xi & 0 & \partial_\xi \\ 0 & \partial_\xi & 0 \end{pmatrix} \begin{pmatrix} e_{1c} \\ e_{r1} \\ e_{1R} \end{pmatrix}, \quad (21)$$

with $e_{1c} = Q/C_2$ and $e_{1R} = R_2\partial_t Q = -R_2 f_1$.

The discretization scheme is shown in Fig. 5, where $j \in \{1, \cdots, N_b\}$ represents the jth element in the x coordinate, and h_1 is the discretization step along the ξ direction. With

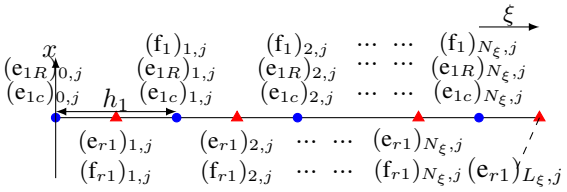

Fig. 5: Discretization schema of (21).

boundary condition $e_{r1}(L_\xi) = 0$, (21) is discretized into:

$$\begin{pmatrix} f_{1d} \\ f_{r1d} \\ f_{1d} \end{pmatrix} = \begin{pmatrix} \mathbf{0} & D_1 & \mathbf{0} \\ -D_1^T & \mathbf{0} & -D_1^T \\ \mathbf{0} & D_1 & \mathbf{0} \end{pmatrix} \begin{pmatrix} e_{1cd} \\ e_{r1d} \\ e_{1Rd} \end{pmatrix} + \begin{pmatrix} \mathbf{0} \\ g_1 \\ \mathbf{0} \end{pmatrix} e_{1b}, \quad (22)$$

with $f_{1d} = \begin{pmatrix} (f_1)_{1,1} & \cdots & (f_1)_{1,N_b} & \cdots & (f_1)_{N_\xi,N_b} \end{pmatrix}^T$, $f_{r1d} = \begin{pmatrix} (f_{r1})_{1,1} & \cdots & (f_{r1})_{1,N_b} & \cdots & (f_{r1})_{N_\xi,N_b} \end{pmatrix}^T$, $e_{1cd} = \begin{pmatrix} (e_{1c})_{1,1} & \cdots & (e_{1c})_{1,N_b} & \cdots & (e_{1c})_{N_\xi,N_b} \end{pmatrix}^T$, $e_{1Rd} = \begin{pmatrix} (e_{1R})_{1,1} & \cdots & (e_{1R})_{1,N_b} & \cdots & (e_{1R})_{N_\xi,N_b} \end{pmatrix}^T$, $e_{1b} = e_{1c}(0) + e_{1Rd}(0)$ and the matrices

$$D_1 = \begin{pmatrix} -\frac{\mathbf{1}}{\mathbf{h_1}} & \frac{\mathbf{1}}{\mathbf{h_1}} & & \\ & \ddots & \ddots & \\ & & \ddots & \frac{\mathbf{1}}{\mathbf{h_1}} \\ & & & -\frac{\mathbf{1}}{\mathbf{h_1}} \end{pmatrix}, g_1 = \begin{pmatrix} -\frac{\mathbf{1}}{\mathbf{h_1}} \\ \mathbf{0} \\ \vdots \\ \mathbf{0} \end{pmatrix},$$

where $R^{N_b \times N_b} \ni \frac{\mathbf{1}}{\mathbf{h_1}} = diag\left(\frac{1}{h_1}\right)$ and $\mathbf{0}$ is zero matrix of appropriate size.

The closure equations $e_{r1} = -f_{r1}/R_1$ and $e_{1R} = -R_2 f_1$ are discretized into:

$$e_{r1d} = L_{r1} f_{r1d}, \text{ and } e_{1Rd} = L_{r2} f_{1d}, \quad (23)$$

with $L_{r1} = diag(-1/R_1)$ and $L_{r2} = diag(-R_2)$.

B. Discretization of the electro-stress diffusion system

Similar to III-A, (18) is recast into:

$$\begin{pmatrix} f_{2d} \\ f_{r2d} \end{pmatrix} = \begin{pmatrix} \mathbf{0} & D_2 \\ -D_2^T & \mathbf{0} \end{pmatrix} \begin{pmatrix} e_{2d} \\ e_{r2d} \end{pmatrix} + \begin{pmatrix} D_{26} & g_2 \\ \mathbf{0} & \mathbf{0} \end{pmatrix} \begin{pmatrix} e_{6d} \\ e_{2b} \end{pmatrix}, \quad (24)$$

where $f_{2d} = \begin{pmatrix} (f_2)_{1,1} & \cdots & (f_2)_{1,N_b} & \cdots & (f_2)_{N_z,N_b} \end{pmatrix}^T$, $f_{r2d} = \begin{pmatrix} (f_{r2})_{1,1} & \cdots & (f_{r2})_{1,N_b} & \cdots & (f_{r2})_{N_z-1,N_b} \end{pmatrix}^T$, $D_{26} = \begin{pmatrix} -M_1 & \cdots & -M_m & \cdots & -M_{Ng} \end{pmatrix}^T$, $R^{N_b \times N_b} \ni M_m = diag\left(-\frac{2Gb}{\mathcal{R}_f L}\left(-\frac{h_2}{2} + \frac{(2m-1)h_2}{2}\right)\right)$, $e_{2b} = \left(-\frac{\lambda}{\sigma_e}\mathbf{j}_e - \lambda_{\mathbf{L}d}\right)$, $\lambda_{\mathbf{L}d} = \begin{pmatrix} {\lambda_{\mathbf{L}}}^1 & \cdots & {\lambda_{\mathbf{L}}}^{N_b} \end{pmatrix}^T$, and matrices

$$D_2 = \begin{pmatrix} \frac{\mathbf{1}}{\mathbf{h_2}} & & \\ -\frac{\mathbf{1}}{\mathbf{h_2}} & \ddots & \\ & \ddots & \frac{\mathbf{1}}{\mathbf{h_2}} \\ & & -\frac{\mathbf{1}}{\mathbf{h_2}} \end{pmatrix}, g_2 = \begin{pmatrix} -\frac{\mathbf{1}}{\mathbf{h_2}} \\ \mathbf{0} \\ \vdots \\ \mathbf{0} \\ \frac{\mathbf{1}}{\mathbf{h_2}} \end{pmatrix}.$$

The closure equation $e_{r2} = -\mathcal{R}_g f_{r2}$ is discretized into

$$e_{r2d} = L_{r3} f_{r2d}, \text{ with } L_{r3} = diag(-\mathcal{R}_g). \quad (25)$$

C. Discretization of the mechanical system

For a clamped-free cantilever beam model, with boundary condition $e_3(L) = e_4(0) = e_5(L) = e_6(0) = 0$, (11) is discretized into:

$$\begin{pmatrix} f_{3d} \\ f_{4d} \\ f_{5d} \\ f_{6d} \end{pmatrix} = \underbrace{\begin{pmatrix} \mathbf{0} & D_3 & \mathbf{0} & S_1 \\ -D_3^T & \mathbf{0} & \mathbf{0} & \mathbf{0} \\ \mathbf{0} & \mathbf{0} & \mathbf{0} & D_3 \\ -S_1^T & \mathbf{0} & -D_3^T & \mathbf{0} \end{pmatrix}}_{J_{md}} \begin{pmatrix} e_{3d} \\ e_{4d} \\ e_{5d} \\ e_{6d} \end{pmatrix} + \underbrace{\begin{pmatrix} \mathbf{0} \\ \mathbf{0} \\ \mathbf{0} \\ -D_{26}^T \end{pmatrix}}_{S_2} e_{2d} + \underbrace{\begin{pmatrix} \mathbf{0} \\ \mathbf{0} \\ \mathbf{0} \\ \text{diag}(\frac{B_p}{L}) \end{pmatrix}}_{S_\lambda} \lambda_{\mathbf{L}d}, \quad (26)$$

where $f_{id} = \begin{pmatrix} f_i^1 & \cdots & f_i^{N_b} \end{pmatrix}^T$, $e_{id} = \begin{pmatrix} e_i^1 & \cdots & e_i^{N_b} \end{pmatrix}^T$, $i = \{3, 4, 5, 6\}$, and matrices

$$D_3 = \begin{pmatrix} \frac{1}{h_3} & & & \\ -\frac{1}{h_3} & \ddots & & \\ & \ddots & \ddots & \\ & & -\frac{1}{h_3} & \frac{1}{h_3} \end{pmatrix}, S_1 = -\begin{pmatrix} \frac{1}{2} & & & \\ \frac{1}{2} & \ddots & & \\ & \ddots & \ddots & \\ & & \frac{1}{2} & \frac{1}{2} \end{pmatrix}.$$

With the coupling relations (13) and (14), closure equations (23) and (25), the discretized subsystems (22), (24) and (26) lead to the global discretized system:

$$\underbrace{\begin{pmatrix} \dot{x}_{1d} \\ \dot{x}_{2d} \\ \dot{x}_{md} \end{pmatrix}}_{\dot{x}_d} = \underbrace{\begin{pmatrix} M_2 D_1^T & P_1 & \mathbf{0} \\ M_1 D_1^T \left(\mathbf{I} - L_{r2} M_2 D_1^T\right) & P_2 & -S_2^T \\ \mathbf{0} & S_2 & J_{md} \end{pmatrix}}_{J_r} \underbrace{\begin{pmatrix} e_{1d} \\ e_{2d} \\ e_{md} \end{pmatrix}}_{e_d} + \underbrace{\begin{pmatrix} \mathbf{0} \\ g_2 \\ S_\lambda \end{pmatrix}}_{g_c} \lambda_{\mathbf{L}d} + \underbrace{\begin{pmatrix} -M_2 g_1 \\ M_1 \left(D_1^T L_{r2} M_2 - \mathbf{I}\right) g_1 \\ \mathbf{0} \end{pmatrix}}_{B} V, \quad (27)$$

with $\mathbf{I}$ the identity matrix of appropriate size,

$$x_{1d} = Q_d, x_{2d} = f_{sd},$$
$$x_{md} = \begin{pmatrix} \partial_x \omega_d - \theta_d & \rho A \partial_t \omega_d & \partial_x \theta_d & \rho I \partial_t \theta_d \end{pmatrix}^T,$$
$$e_d = L_d x_d, L_d = diag\left(1/C_2, \mathcal{R}_f, GA, 1/(\rho A), EI, 1/(\rho I)\right),$$
$$M_1 = g_2 \frac{\lambda}{\sigma_e L b} g_1^T L_{r1}, P_1 = M_2 g_1 \frac{\lambda}{\sigma_e L b} g_2^T,$$
$$M_2 = -\left(\mathbf{I} + D_1 L_{r1} D_1^T L_{r2}\right)^{-1} D_1 L_{r1}, \text{ and}$$
$$P_2 = -D_2 L_{r3} D_2 - M_1 \left(D_1^T L_{r2} M_2 + \mathbf{I}\right) g_1 \frac{\lambda}{\sigma_e L b} g_2^T.$$

The geometric constraint in (20) becomes $g_c^T e_d = 0$.

D. Elimination of the Lagrange multiplier

The Lagrange multiplier $\lambda_{\mathbf{L}d}$ in (27) has to be eliminated in order to perform the simulation and apply the control strategies afterwards. The proposed method is based on the coordinate projection in [22] that preserves the PH structure of the system. This projection approach has later been improved in [23] to

get a descriptor formulation in the linear case, which finally leads to:

$$\begin{pmatrix} \mathbf{I} & \mathbf{0} \\ \mathbf{0} & \mathbf{0} \end{pmatrix} \begin{pmatrix} \dot{\tilde{X}}_1 \\ \dot{\tilde{X}}_2 \end{pmatrix} = \begin{pmatrix} \tilde{J}_{11} & \tilde{J}_{12} \\ g_c^T \tilde{M}^T \end{pmatrix} \tilde{L}_d \begin{pmatrix} \tilde{X}_1 \\ \tilde{X}_2 \end{pmatrix} + \tilde{M} B V, \quad (28)$$

where $\tilde{M}$ is the coordinate transformation matrix such that $\tilde{M} = \begin{pmatrix} S \\ (g_c^T g_c)^{-1} g_c^T \end{pmatrix}$ with S satisfying $S \cdot g_c = 0$. $\tilde{X}_1 = \tilde{M} \begin{pmatrix} x_{1d}^T & x_{2d}^T & x_{3d}^T & x_{4d}^T & x_{5d}^T \end{pmatrix}^T$, $\tilde{X}_2 = \tilde{M} x_{6d}^T$, $\tilde{J} = \begin{pmatrix} \tilde{J}_{11} & \tilde{J}_{12} \\ \tilde{J}_{21} & \tilde{J}_{22} \end{pmatrix} = \tilde{M} J_r \tilde{M}^T$, and $\tilde{L}_d = \tilde{M}^{-T} L_d \tilde{M}^{-1}$.

IV. Simulation Results and Experimental Validation

The experimental set-up is shown in Fig. 6. The IPMC patch is controlled through a computer equipped with a dSPACE controller board in order to generate different types of input voltages. The amplifier is used to regulate the input voltage. The laser position sensor and current sensor are dedicated to the measure of the tip displacement of the IPMC and to the measure of the output current, respectively. The dimension of the considered Nafion-based IPMC actuator is $45\text{mm} \times 5\text{mm} \times 0.2\text{mm}$, with a density of $1.633 \times 10^3 \text{kg/m}^3$, Young's modulus of $9 \times 10^7 \text{Pa}$ and Poisson ratio of 0.3. According to [24], $\phi = 0.34$ and $\eta = 0.010 \text{Pa} \cdot \text{s}$. Identified parameters are listed in Table I, where $R_{1\text{total}}$, $R_{2\text{total}}$ and $C_{2\text{total}}$ are the identified resistances and capacitance of the electrodes.

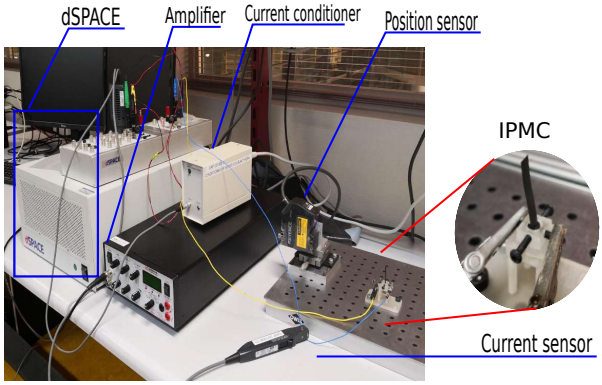

Fig. 6: Experimental setup of IPMC.

TABLE I: Identified parameters.

$R_{1\text{total}}$	460.54	Ω	λ	16.6×10^{-9}	$\text{m}^2/(\text{Vs})$
$R_{2\text{total}}$	3	Ω	σ_e	13.10	$1/(\Omega\text{m})$
$C_{2\text{total}}$	0.021	F	d	10	nm

The temporal evolution of the current obtained in the simulation with a step voltage of 1V are depicted and compared to the experimental one in Fig. 7. The simulations correspond to four values of N_ξ (10, 50, 100 and 200), while both N_z and N_b fixed to 10. As N_ξ increases, the peak response obtained in simulation approaches gradually the experimental one (marked by black solid line), while the settling time remains similar. This evolution is in accordance with the frequency responses

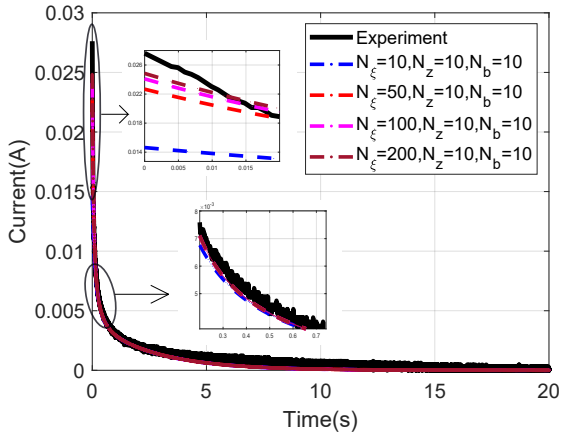

Fig. 7: Variation of the output current according to different discretization numbers N_ξ, compared with experimental data.

of the transfer functions associated to different values of N_ξ.

From the Bode diagram in Fig. 8, the transfer functions have a similar shape at low frequencies but are slightly different for the high frequencies. This difference tends to zero when N_ξ tends to infinity. However, one can notice that for the considered example, the difference is minor for N_ξ greater than 50. The influence of N_z and N_b on the current has also been investigated but omitted in this paper for the sake of brevity. Actually, these parameters have a minor effect on the current responses compared to that of N_ξ.

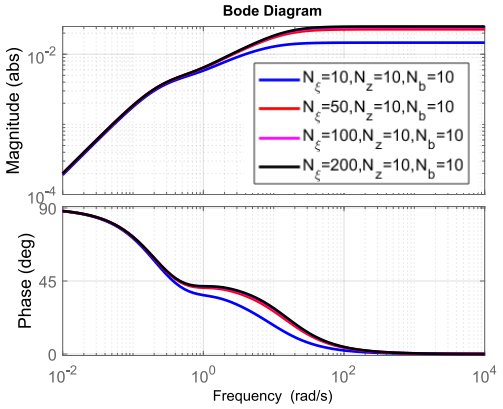

Fig. 8: Bode diagrams for different discretization configurations of the electrical system.

We consider now the consistency between the simulation and experimental results for the tip deflection of the IPMC strip. Preliminary works suggest that the deflection does not change with N_z. Meanwhile, its variation is negligible as soon as N_ξ is greater than 20. As a consequence, the influence of the discretization number N_b on the mechanical deformation is demonstrated for : $N_\xi = 50$ and $N_z = 10$. As shown in Fig. 9, N_b has a significant influence on the predicted response: the simulation results of the tip deflection approach to the experimental ones with the increase of the discretization number N_b. One can see that $N_b = 100$ leads to a very good approximation of the system behavior. This demand of a large discretization number is mainly due to the applied

finite differences method, because this method is a direct approximation of the PDEs, and one needs a great number of elements to approximate the analytic solutions.

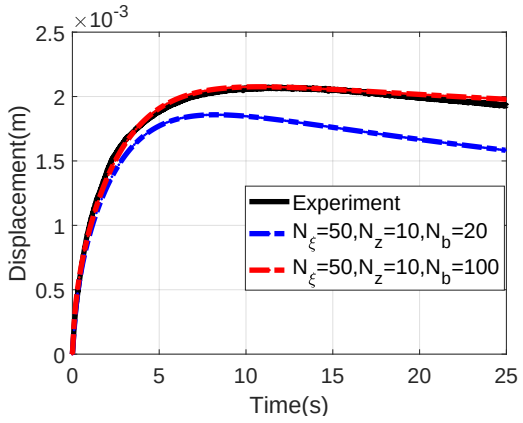

Fig. 9: Tip deflection of IPMC strip according to different discretization numbers N_b, compared with experimental data.

The two bending moments generated by the gel are simulated in Fig. 10 for $N_\xi = 50$, $N_z = 10$ and $N_b = 100$. Fig. 10a shows the distribution along the beam and the temporal evolution of the bending moment M_{x1}, while Fig. 10b shows those related to M_{x2}. At each time, the bending moments M_{x1} are the same whatever the points along the beam. Nevertheless, as illustrated by the dashed light blue line in Fig. 10b, M_{x2} has a larger value at the clamped point and is equal to zero at the free end point, which is in accordance with the considered boundary conditions for the cantilever.

The sum of the M_{x1} and M_{x2} forms the total bending moment that applies to the beam model, whose simulation result is given in Fig. 10c. One can notice a diffusion phenomenon in Fig. 10, as illustrated by the red solid lines. This diffusion effect of the bending moment explains the back-relaxation of the displacement in our model, as shown in Fig. 9. Considered as the main drawback of such actuators, this back relaxation exists in almost all Nafion-based IPMCs. More thorough studies on this phenomenon are referred to some recent references, e.g. [25].

A comparison between the experimental and simulation results in the case of a sinusoidal input voltage of amplitude 1V and frequency of 1Hz is also given in Fig. 11. One can see the simulation results are consistent with the experimental ones. It also illustrates that the proposed model copes with the hysteretic behavior of the actuator.

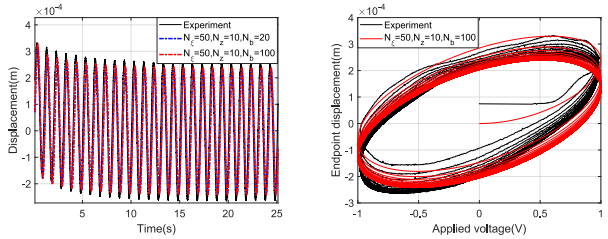

Fig. 11: Tip deflection of IPMC strip with a sinusoidal input voltage.

Remark 2. *Comparisons have also been carried out between homogeneous and irregular meshing. The results show that one can reduce the number of elements near the clamped side without modifying significantly the behavior of the system. Furthermore, the order of the overall system can be drastically reduced using finite elements methods [23] rather than finite differences.*

V. First modeling of 2D IPMC actuated structure

We consider here a simplified model of a 2D IPMC actuated structure stemming from the modeling of a flexible medical endoscope. The conceptual figure of such system is illustrated in Fig. 12. The endoscope is modeled as a thin elastic shell in a cylindrical coordinate with three directions X, Θ and α_3. α_3 is normal to the reference surface generated by X and Θ under the assumption that $\alpha_3/a \ll 1$ (a denotes the cylinder radius). The IPMC actuator strip is assumed to have bending deformation only in the radial direction, and the deformation is supposed to be symmetric. As a consequence, comparing to the endoscope, the IPMC strip can be simplified as a 1D string line, as shown in Fig.12b.

A. Thin elastic cylinder shell model in port-Hamiltonian formulation

For linear thin elastic shell structure, there exists several models under different assumptions [26]. The interested reader can find in [27]–[29] a detailed review of these models. Among these models, Love's theory is mostly applied and based on the following assumptions:

1) Deformations are small, and Hooke's law applies.
2) The material of the shell is orthotropic.
3) The cross section of the referenced surface remains unstretched.
4) The cross section of the referenced surface remains normal after deformation, so there is no shear deformation.
5) The rotatory inertia is neglected .

Models using Love's theory have a distinct inaccuracy when the wavelength of the bending waves is short compared to the thickness of the shell, where the shear deformation and the rotatory inertia become influential [30]. To deal with this issue, Soedel released the assumptions 4 and 5 of Love's theory, and proposed a modified model in [31]. In this section we use this Soedel's model for the model of the endoscope. u_{XX}, $u_{\Theta\Theta}$ and w represent the deformations in X, Θ and α_3 directions, respectively. β_X and β_Θ relate to the rotations of tangents to the reference surface oriented along the coordinates X and Θ [32]. According to assumption 3, the displacements are composed of u_{XX}, $u_{\Theta\Theta}$, W, β_X and β_Θ. The relations between strains and displacements are[3]:

$$\epsilon_{XX} = \epsilon^0_{XX} + \alpha_3 k_{XX}, \qquad \epsilon_{\Theta\Theta} = \epsilon^0_{\Theta\Theta} + \alpha_3 k_{\Theta\Theta},$$
$$\gamma_{X3} = \frac{\partial W}{\partial X} + \beta_X, \qquad \gamma_{\Theta 3} = -\frac{u_{\Theta\Theta}}{a} + \frac{1}{a}\frac{\partial W}{\partial \Theta} + \beta_\Theta,$$
$$\gamma_{X\Theta} = \gamma^0_{X\Theta} + \alpha_3 k_{X\Theta},$$

[3]Readers are suggested to [33] and [32] for detailed calculations.

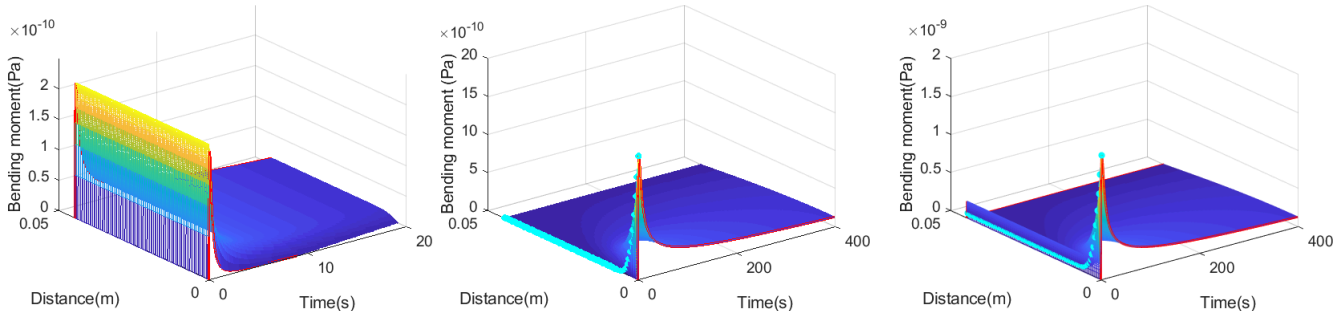

(a) M_{x1} (b) M_{x2} (c) M_{ext}

Fig. 10: Simulation results for M_{x1}, M_{x2} and M_{ext} along x-axis and the time ($N_\xi = 50, N_z = 10$ and $N_b = 100$).

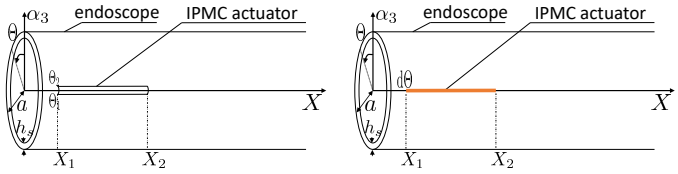

(a) (b)

Fig. 12: Conceptual figure of endoscope attached with IPMC actuator.

where ϵ^0_{XX}, $\epsilon^0_{\Theta\Theta}$ and $\gamma^0_{X\Theta}$ are the membrane strains, and where k_{XX}, $k_{\Theta\Theta}$ and $k_{X\Theta}$ are curvature terms that are formulated as:

$$\epsilon^0_{XX} = \frac{\partial u_{XX}}{\partial X}, \qquad \epsilon^0_{\Theta\Theta} = \frac{1}{a}\left(\frac{\partial u_{\Theta\Theta}}{\partial \Theta} + W\right),$$
$$\gamma^0_{X\Theta} = \frac{\partial u_{\Theta\Theta}}{\partial X} + \frac{1}{a}\frac{\partial u_{XX}}{\partial \Theta}, k_{XX} = \frac{\partial \beta_X}{\partial X},$$
$$k_{\Theta\Theta} = \frac{1}{a}\frac{\partial \beta_\Theta}{\partial \Theta}, \qquad k_{X\Theta} = \frac{\partial \beta_\Theta}{\partial X} + \frac{1}{a}\frac{\partial \beta_X}{\partial \Theta}.$$

The resultant forces and moments are calculated as:

$$N_{XX} = K_s\left(\epsilon^0_{XX} + \nu_s\epsilon^0_{\Theta\Theta}\right), N_{\Theta\Theta} = K_s\left(\epsilon^0_{\Theta\Theta} + \nu_s\epsilon^0_{XX}\right),$$
$$N_{X\Theta} = K_s\frac{1-\nu_s}{2}\gamma^0_{X\Theta}, \qquad M_{XX} = D_s\left(k_{XX} + \nu_s k_{\Theta\Theta}\right),$$
$$M_{\Theta\Theta} = D_s\left(k_{\Theta\Theta} + \nu_s k_{XX}\right), M_{X\Theta} = D_s\frac{1-\nu_s}{2}k_{X\Theta},$$
$$Q_{X3} = k' G_s h_s \gamma_{X3}, \qquad Q_{\Theta 3} = k' G_s h_s \gamma_{\Theta 3}, \tag{29}$$

where $K_s = E_s h_s/\left(1-\nu_s^2\right)$, and $D_s = E_s h_s^3/12\left(1-\nu_s^2\right)$, h_s is the thickness of the shell, ν_s, E_s, k' and G_s denote the Poisson ratio, Young's modulus, shear coefficient, and shear modulus of the cylindrical shell, respectively. The dynamic equations of the cylindrical shell are given by [31]:

$$\rho_s h_s\frac{\partial^2 u_{XX}}{\partial t^2} = \frac{\partial N_{XX}}{\partial X} + \frac{1}{a}\frac{\partial N_{X\Theta}}{\partial \Theta},$$
$$\rho_s h_s\frac{\partial^2 u_{\Theta\Theta}}{\partial t^2} = \frac{\partial N_{X\Theta}}{\partial X} + \frac{1}{a}\frac{\partial N_{\Theta\Theta}}{\partial \Theta} + \frac{1}{a}Q_{\Theta 3},$$
$$\rho_s h_s\frac{\partial^2 w}{\partial t^2} = \frac{\partial Q_{X3}}{\partial X} + \frac{1}{a}\frac{\partial Q_{\Theta 3}}{\partial \Theta} - \frac{1}{a}N_{\Theta\Theta},$$
$$\frac{\rho_s h_s^3}{12}\frac{\partial^2 \beta_X}{\partial t^2} = \frac{\partial M_{XX}}{\partial X} + \frac{1}{a}\frac{\partial M_{X\Theta}}{\partial \Theta} - Q_{X3} + m_X,$$
$$\frac{\rho_s h_s^3}{12}\frac{\partial^2 \beta_\Theta}{\partial t^2} = \frac{\partial M_{X\Theta}}{\partial X} + \frac{1}{a}\frac{\partial M_{\Theta\Theta}}{\partial \Theta} - Q_{\Theta 3}, \tag{30}$$

where m_X is the external bending moment density.

In order to reformulate the above dynamical equations under the PHS framework, we define the following flow, state and effort variables as [34]:

$$f_{cy} = \frac{\partial x_{cy}}{\partial t} = \frac{\partial}{\partial t}\begin{pmatrix}\rho_s h_s\frac{\partial \mathbf{u}}{\partial t}\\ \rho_s h_s\frac{\partial W}{\partial t}\\ \frac{\rho_s h_s^3}{12}\frac{\partial \boldsymbol{\beta}}{\partial t}\\ \mathbb{k}\\ \mathbb{A}\\ \boldsymbol{\gamma}\end{pmatrix}, e_{cy} = \begin{pmatrix}\frac{\partial \mathbf{u}}{\partial t}\\ \frac{\partial W}{\partial t}\\ \frac{\partial \boldsymbol{\beta}}{\partial t}\\ \mathbb{M}\\ \mathbb{N}\\ \mathbf{Q}\end{pmatrix}, \tag{31}$$

with vectors

$$\mathbf{u} = \begin{pmatrix}u_{XX}\\ u_{\Theta\Theta}\end{pmatrix}, \boldsymbol{\beta} = \begin{pmatrix}\beta_X\\ \beta_\Theta\end{pmatrix}, \boldsymbol{\gamma} = \begin{pmatrix}\gamma_{X3}\\ \gamma_{\Theta 3}\end{pmatrix}, \mathbf{Q} = \begin{pmatrix}Q_{X3}\\ Q_{\Theta 3}\end{pmatrix},$$

and second order tensors

$$\mathbb{k} = \begin{pmatrix}k_{XX} & k_{X\Theta}\\ k_{X\Theta} & k_{\Theta\Theta}\end{pmatrix}, \mathbb{A} = \begin{pmatrix}\epsilon^0_{XX} & \gamma^0_{X\Theta}\\ \gamma^0_{X\Theta} & \epsilon^0_{\Theta\Theta}\end{pmatrix},$$
$$\mathbb{M} = \begin{pmatrix}M_{XX} & M_{X\Theta}\\ M_{X\Theta} & M_{\Theta\Theta}\end{pmatrix}, \mathbb{N} = \begin{pmatrix}N_{XX} & N_{X\Theta}\\ N_{X\Theta} & N_{\Theta\Theta}\end{pmatrix}.$$

The dynamic equations (30) over the 2D cylindrical domain $\Omega = [0, L_s] \times [0, 2\pi]$ can be reformulated into the following PHS:

$$f_{cy} = \mathcal{J}_{cy}e_{cy} + B_{cy}m_X, \tag{32}$$

with

$$\mathcal{J}_{cy} = \begin{pmatrix}0 & 0 & 0 & 0 & Div & \mathfrak{a}\\ 0 & 0 & 0 & 0 & -\mathfrak{a}: & div\\ 0 & 0 & 0 & Div & 0 & -1\\ 0 & 0 & Grad & 0 & 0 & 0\\ Grad & \mathfrak{a} & 0 & 0 & 0 & 0\\ -\mathfrak{a} & grad & 1 & 0 & 0 & 0\end{pmatrix},$$
$$\mathfrak{a} = \begin{pmatrix}0 & 0\\ 0 & \frac{1}{a}\end{pmatrix}, B_{cy} = \begin{pmatrix}\mathbf{0}^T & 0 & \begin{pmatrix}1 & 0\end{pmatrix} & \bar{\bar{0}} & \bar{\bar{0}} & \mathbf{0}^T\end{pmatrix}^T,$$

where $\bar{\bar{0}}$ is a second order tensor of zero, Div and div represent the divergence operators for tensors and vectors, $Grad$ and $grad$ denote the gradient operators for vectors and scalars, and

: is the double dot product for tensors. The time derivative of the Hamiltonian is formulated as [34]:

$$\begin{aligned}\frac{\mathrm{d}H_{cy}}{\mathrm{d}t} &= \int_\Omega \left(f_{cy}^T e_{cy}\right)\mathrm{d}\Omega \\ &= \int_\Omega \left(Div\left(\mathbb{N}\right)\frac{\partial \mathbf{u}}{\partial t} + Grad\left(\frac{\partial \mathbf{u}}{\partial t}\right) : \mathbb{N} + div\left(\mathbf{Q}\right)\frac{\partial W}{\partial t} \right. \\ &\quad \left. + grad\left(\frac{\partial W}{\partial t}\right)\mathbf{Q} + Div\left(\mathbb{M}\right)\frac{\partial \boldsymbol{\beta}}{\partial t} + Grad\left(\frac{\partial \boldsymbol{\beta}}{\partial t}\right) : \mathbb{M}\right)\mathrm{d}\Omega \\ &= \int_{\partial\Omega} \left(\frac{\partial W}{\partial t}\left(\mathbf{Q}\cdot\mathbf{n}\right) + \left(\mathbb{N} : \left(\mathbf{n}\otimes\mathbf{n}\right)\right)\left(\frac{\partial \mathbf{u}}{\partial t}\cdot\mathbf{n}\right)\right. \\ &\quad + \left(\frac{\partial \mathbf{u}}{\partial t}\cdot\mathbf{s}\right)\left(\mathbb{N} : \left(\mathbf{s}\otimes\mathbf{n}\right)\right) + \left(\mathbb{M} : \left(\mathbf{n}\otimes\mathbf{n}\right)\right)\left(\frac{\partial \boldsymbol{\beta}}{\partial t}\cdot\mathbf{n}\right) \\ &\quad \left. + \left(\frac{\partial \boldsymbol{\beta}}{\partial t}\cdot\mathbf{s}\right)\left(\mathbb{M} : \left(\mathbf{s}\otimes\mathbf{n}\right)\right)\right)\mathrm{d}s, \end{aligned} \tag{33}$$

with $\partial\Omega = (0,\Theta)\cup(L_s,\Theta)$ boundaries of domain Ω, $\otimes$ the tensor product, $\mathbf{n}$ and $\mathbf{s}$ the normal and tangent unit vector with respect to the boundaries, respectively.

With the fact that the shell is closed and in a cylindrical coordinate, we take $\mathbf{n} = \begin{pmatrix}1\\0\end{pmatrix}$, and $\mathbf{s} = \begin{pmatrix}0\\1\end{pmatrix}$, leading to:

$$\begin{aligned}&\frac{\partial \mathbf{u}}{\partial t}\cdot\mathbf{n} = \frac{\partial u_{XX}}{\partial t}, \frac{\partial \mathbf{u}}{\partial t}\cdot\mathbf{s} = \frac{\partial u_{\Theta\Theta}}{\partial t}, \frac{\partial \boldsymbol{\beta}}{\partial t}\cdot\mathbf{n} = \frac{\partial \beta_X}{\partial t}, \\ &\frac{\partial \boldsymbol{\beta}}{\partial t}\cdot\mathbf{s} = \frac{\partial \beta_\Theta}{\partial t}, \mathbf{Q}\cdot\mathbf{n} = Q_{X3}, \mathbb{N} : \left(\mathbf{n}\otimes\mathbf{n}\right) = N_{XX}, \\ &\mathbb{N} : \left(\mathbf{s}\otimes\mathbf{n}\right) = N_{X\Theta}, \mathbb{M} : \left(\mathbf{n}\otimes\mathbf{n}\right) = M_{XX}, \\ &\mathbb{M} : \left(\mathbf{s}\otimes\mathbf{n}\right) = M_{X\Theta},\end{aligned}$$

The boundary port variables are calculated according to the time derivative of Hamiltonian (33) as:

$$f_\partial = \begin{pmatrix}\frac{\partial W}{\partial t}\\ \frac{\partial u_{XX}}{\partial t}\\ \frac{\partial u_{\Theta\Theta}}{\partial t}\\ \frac{\partial \beta_X}{\partial t}\\ \frac{\partial \beta_\Theta}{\partial t}\end{pmatrix}\left(0/L_s,\Theta\right), e_\partial = \begin{pmatrix}Q_{X3}\\ N_{XX}\\ N_{X\Theta}\\ M_{XX}\\ M_{X\Theta}\end{pmatrix}\left(0/L_s,\Theta\right).$$

B. Mechanical coupling between the endoscope and the IPMC actuator

We assume that the interconnection of the IPMC and the endoscope is perfect such that the mechanical deformation of the IPMC is considered as the same as the one of the endoscope. The interconnection between the gel and the endoscope is then written as:

$$\begin{pmatrix}\dot{f}_s\\ f_{r2}\\ f_{cy}\end{pmatrix} = \begin{pmatrix}\begin{pmatrix}0 & \partial_z\\ \partial_z & 0\end{pmatrix} & \mathcal{J}_{inter}\\ -\mathcal{J}_{inter}^* & \mathcal{J}_{cy}\end{pmatrix}\begin{pmatrix}e_2\\ \mathcal{R}_g\partial_z\left(\mathcal{R}_f f_s\right)\\ e_{cy}\end{pmatrix} + A_L\lambda_{\mathbf{L}},$$

where

$$\mathcal{J}_{inter} = \begin{pmatrix}0 & 0 & \left(-B_a f\mathbb{1}_z & 0\right) & 0 & 0 & 0\\ 0 & 0 & 0 & & 0 & 0 & 0\end{pmatrix},$$

$$A_L = \begin{pmatrix}-\partial_Z\mathbb{1}_z\\ 0\\ B_{cy}B_p f\end{pmatrix}, f = \begin{cases}\frac{1}{X_2-X_1}, \text{for } X\in(X_1,X_2),\\ 0, \text{otherwise.}\end{cases}$$

The constraint arising from the coupling is given by

$$e_2\left(-\frac{h}{2}\right) - e_2\left(-\frac{h}{2}\right) - B_p f\frac{\partial \beta_X}{\partial t} = 0,$$

which is similar to (20).

To complete this model, we have to take into account the coupling between the electrical system and electro-stress diffusion system (gel) which is exactly the same as the one of Fig. 3 and is omitted in the interest of space.

VI. Conclusion

In this paper a detailed model of an IPMC patch is established under the constrained port-Hamiltonian framework. The Lagrange multiplier method is used to deal with the geometric constraints arising from the interconnection of the gel with the actuator electrode. The global system is associated with a Stokes-Dirac structure, stemming from the expression of energy balances. The system is discretized by means of the finite differences method on staggered grids and is further reduced to a set of differential algebraic equations, for the purpose of facilitating the numerical simulation and preserving its geometric structure. Finally, experiments and simulations are carried out with a step case as well as a sinusoidal case. It has been shown how to choose different discretization parameters such that the simulations of the output current and displacement at the endpoint of the IPMC patch match with the experimental data. In a second instance, a simplified model of a 2D flexible structure equipped with an IPMC patch is proposed. It is shown that one can use the same interconnection and Lagrange multipliers to derive a physically consistent model of the overall actuated system. In future works we first intend to relax the quite stringent assumption in the 2D case in order to get a more realistic model suitable for control design for realistic flexible actuated endoscopes. After considering structure preserving model order reduction this reduced order model will then be used for energy based control design.

References

[1] M. Shahinpoor and K. J. Kim, "Ionic polymer–metal composites: Iv. industrial and medical applications," *Smart materials and structures*, vol. 14, no. 1, pp. 197–214, 2004.

[2] J. Wang, A. J. McDaid, C. Z. Lu, and K. C. Aw, "A compact ionic polymer-metal composite (IPMC) actuated valveless pump for drug delivery," *IEEE/ASME Transactions on Mechatronics*, vol. 22, no. 1, pp. 196–205, 2017.

[3] K. Park, M.-K. Yoon, S. Lee, J. Choi, and M. Thubrikar, "Effects of electrode degradation and solvent evaporation on the performance of ionic-polymer–metal composite sensors," *Smart Materials and Structures*, vol. 19, no. 7, p. 075002, 2010.

[4] Y. Xiao and K. Bhattacharya, "Modeling electromechanical properties of ionic polymers," in *Smart Structures and Materials 2001: Electroactive Polymer Actuators and Devices*, vol. 4329. International Society for Optics and Photonics, 2001, pp. 292–301.

[5] K. M. Newbury and D. J. Leo, "Electromechanical modeling and characterization of ionic polymer benders," *Journal of Intelligent Material Systems and Structures*, vol. 13, no. 1, pp. 51–60, 2002.

[6] J. Khawwaf, J. Zheng, R. Chai, R. Lu, and Z. Man, "Adaptive microtracking control for an underwater IPMC actuator using new hyperplane-based sliding mode," *IEEE/ASME Transactions on Mechatronics*, vol. 24, no. 5, pp. 2108–2117, 2019.

[7] M. Shahinpoor, "Micro-electro-mechanics of ionic polymeric gels as electrically controllable artificial muscles," *Journal of Intelligent Material Systems and Structures*, vol. 6, no. 3, pp. 307–314, 1995.

[8] S. Nemat-Nasser and J. Y. Li, "Electromechanical response of ionic polymer-metal composites," *Journal of Applied Physics*, vol. 87, no. 7, pp. 3321–3331, 2000.

[9] P. C. Branco and J. Dente, "Derivation of a continuum model and its electric equivalent-circuit representation for ionic polymer–metal composite (IPMC) electromechanics," *Smart Materials and Structures*, vol. 15, no. 2, p. 378, 2006.
[10] R. Kanno, S. Tadokoro, T. Takamori, M. Hattori, and K. Oguro, "Modeling of icpf (ionic conducting polymer film) actuator-modeling of electrical characteristics," in *Industrial Electronics, Control, and Instrumentation, 1995., Proceedings of the 1995 IEEE IECON 21st International Conference on*, vol. 2. IEEE, 1995, pp. 913–918.
[11] K. M. Newbury and D. J. Leo, "Linear electromechanical model of ionic polymer transducers-part i: Model development," *Journal of Intelligent Material Systems and Structures*, vol. 14, no. 6, pp. 333–342, 2003.
[12] Z. Chen and X. Tan, "A control-oriented and physics-based model for ionic polymer–metal composite actuators," *IEEE/ASME Transactions on Mechatronics*, vol. 13, no. 5, pp. 519–529, 2008.
[13] G. Nishida, K. Takagi, B. Maschke, and T. Osada, "Multi-scale distributed parameter modeling of ionic polymer-metal composite soft actuator," *Control Engineering Practice*, vol. 19, no. 4, pp. 321–334, 2011.
[14] M. Shahinpoor, Ed., *Ionic Polymer Metal Composites (IPMCs)*, ser. Smart Materials Series. The Royal Society of Chemistry, 2016, vol. 1.
[15] Y. Le Gorrec, H. Zwart, and B. Maschke, "Dirac structures and boundary control systems associated with skew-symmetric differential operators," *SIAM journal on control and optimization*, vol. 44, no. 5, pp. 1864–1892, 2005.
[16] J. Villegas, "A port-Hamiltonian approach to distributed parameter systems," Ph.D. dissertation, University of Twente, Netherlands, 5 2007.
[17] Z. Zhu, H. Chen, Y. Wang, and B. Li, "Multi-physical modeling for electro-transport and deformation of ionic polymer metal composites," in *Electroactive Polymer Actuators and Devices (EAPAD) 2012*, vol. 8340. International Society for Optics and Photonics, 2012, p. 83400Q.
[18] T. Yamaue, H. Mukai, K. Asaka, and M. Doi, "Electrostress diffusion coupling model for polyelectrolyte gels," *Macromolecules*, vol. 38, no. 4, pp. 1349–1356, 2005.
[19] P. De Gennes, K. Okumura, M. Shahinpoor, and K. J. Kim, "Mechano-electric effects in ionic gels," *EPL (Europhysics Letters)*, vol. 50, no. 4, p. 513, 2000.
[20] A. Macchelli and C. Melchiorri, "Modeling and Control of the Timoshenko Beam. The Distributed Port Hamiltonian Approach," *SIAM Journal on Control and Optimization*, vol. 43, no. 2, pp. 743–767, 2004.
[21] V. Trenchant, H. Ramirez, Y. Le Gorrec, and P. Kotyczka, "Finite differences on staggered grids preserving the port-Hamiltonian structure with application to an acoustic duct," *Journal of Computational Physics*, vol. 373, pp. 673–697, 2018.
[22] A.J. van der Schaft and B. Maschke, "On the Hamiltonian formulation of nonholonomic mechanical systems," *Reports on Mathematical Physics*, vol. 34, no. 2, pp. 225 – 233, 1994.
[23] Y. Wu, B. Hamroun, Y. Le Gorrec, and B. Maschke, "Port Hamiltonian system in descriptor form for balanced reduction: Application to a nanotweezer," *IFAC Proceedings Volumes*, vol. 47, no. 3, pp. 11 404–11 409, 2014.
[24] J. W. Paquette, K. J. Kim, J.-D. Nam, and Y. S. Tak, "An equivalent circuit model for ionic polymer-metal composites and their performance improvement by a clay-based polymer nano-composite technique," *Journal of Intelligent Material Systems and Structures*, vol. 14, no. 10, pp. 633–642, 2003.
[25] M. Porfiri, H. Sharghi, and P. Zhang, "Modeling back-relaxation in ionic polymer metal composites: The role of steric effects and composite layers," *Journal of Applied Physics*, vol. 123, no. 1, p. 014901, 2018.
[26] A. Farshidianfar and P. Oliazadeh, "Free vibration analysis of circular cylindrical shells: comparison of different shell theories," *International Journal of Mechanics and Applications*, vol. 2, no. 5, pp. 74–80, 2012.
[27] A. W. Leissa, *Vibration of shells*. Scientific and Technical Information Office, National Aeronautics and Space Administration, 1973, vol. 288.
[28] M. S. Qatu, "Recent research advances in the dynamic behavior of shells: 1989-2000, Part 1: Laminated composite shells ," *Applied Mechanics Reviews*, vol. 55, no. 4, pp. 325–350, 07 2002. [Online]. Available: https://doi.org/10.1115/1.1483079
[29] ——, "Recent research advances in the dynamic behavior of shells: 1989–2000, Part 2: Homogeneous shells ," *Applied Mechanics Reviews*, vol. 55, no. 5, pp. 415–434, 09 2002. [Online]. Available: https://doi.org/10.1115/1.1483078
[30] U. Kristiansen, W. Soedel, and J. Hamilton, "An investigation of scaling laws for vibrating beams and plates with special attention to the effects of shear and rotatory inertia," *Journal of Sound and Vibration*, vol. 20, no. 1, pp. 113–122, 1972.
[31] W. Soedel, "On the vibration of shells with timoshenko-mindlin type shear deflections and rotatory inertia," *Journal of Sound and Vibration*, vol. 83, no. 1, pp. 67–79, 1982.
[32] H. Kraus, *Thin elastic shells: an introduction to the theoretical foundations and the analysis of their static and dynamic behavior*. John Wiley & Sons, 1967.
[33] I. S. Sokolnikoff, R. D. Specht *et al.*, *Mathematical theory of elasticity*. McGraw-Hill New York, 1956, vol. 83.
[34] A. Brugnoli, D. Alazard, V. Pommier-Budinger, and D. Matignon, "Port-Hamiltonian formulation and symplectic discretization of plate models part i: Mindlin model for thick plates," *Applied Mathematical Modelling*, vol. 75, pp. 940–960, 2019.

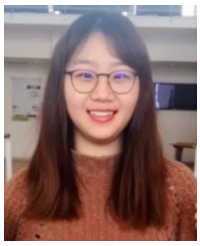

Ning Liu was born in Heze, China in 1995. She received her bachelor degree in aircraft design and engineering from the Northwestern Polytechnical University, Xi'an, China in 2016 and her engineer degree (equivalent of master degree) in mechanical engineering from the national institute of applied sciences (INSA, Lyon, France) in 2017. Since 2017, she is a Ph.D. student of automatic control in University of Bourgogne Franche-Comté, and affiliated to the AS2M department at FEMTO-ST institute (UMR CNRS 6174) in Besançon, France. Her research interests include electro-active polymer actuators, port-Hamiltonian systems, structure preserving discretization and passivity-based control.

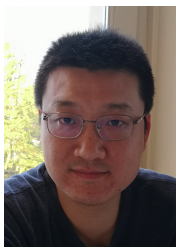

Yongxin Wu was born in Baoji, China in 1985. He received his engineer degree in Transportation Information and Control from the University of Chang'an, Xi'an, China in 2010 and his Master degree in Automatic Control from the University Claude Bernard of Lyon, Villeurbanne, France in 2012. He received his Ph.D. degree in Automatic Control in 2015 for his work on the model and controller reduction of port Hamiltonian systems at the Laboratory of Control and Chemical Engineering (LAGEP UMR CNRS 5007) of the University Claude Bernard of Lyon, Villeurbanne, France. From 2015 to 2016, He held a post-doctoral and teaching assistant position at LAGEP. Since 2016, he is an Associate Professor of Automatic Control at National Engineering Institute in Mechanics and Microtechnologies and affiliated to the AS2M department at FEMTO-ST institute (UMR CNRS 6174) in Besançon, France. His research interests include port Hamiltonian systems, model and controller reduction, modelling and control of multi-physical systems.

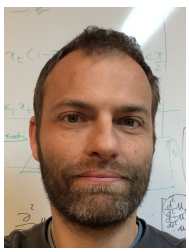

Yann Le Gorrec was graduated as engineer in "Control, Electronics, Computer Engineering" at the National Institute of Applied Sciences (INSA, Toulouse, France) in 1995. He received his Ph. D. degree from the National Higher School of Aeronautics and Aerospace (Supaero, Toulouse, France) in 1998. His field of interest was robust and self-scheduled control design. From 1999 to 2008, he was Associate Professor in Automatic Control at the Laboratory of Control and Chemical Engineering of Lyon Claude Bernard University (LAGEP, Villeurbanne, France). He worked the modeling and control of irreversible and distributed parameter systems with an application to physico-chemical processes. From september 2008 he is Professor at National Engineering Institute in Mechanics and Microtechnologies, and affiliated to the FEMTO-ST institute (UMR CNRS 6174), Besanç on, France. His main research activity is on port Hamiltonian formulations and their use for the modeling of multi-physical systems, model reduction, and control of non-linear and distributed parameter systems.